RESEARCH ARTICLE
doi: 10.2306/scienceasia1513-1874.2026.072

ScienceAsia 52 (4): 2026: ID 2026072: **1–9**

Interfacial modification of epoxy-coated coal gangue proppants using silane coupling agent

Xiaoyang Liu[a], **Dongyan Fan**[a], **Zhongquan Feng**[b], **Wei Liu**[a], **Jianbin Song**[a,*], **Yu Li**[b,*]

[a] Xinjiang Key Laboratory for Value-added Utilization of Heavy Carbon Resources, School of Chemistry and Chemical Engineering, Yili Normal University, Yining 835000 China

[b] State Key Laboratory of Advanced Metallurgy, University of Science and Technology Beijing, Beijing 100083 China

*Corresponding authors, e-mail: jianbin1102@163.com, leeuu00@sina.com

Received 16 Oct 2025, Accepted 7 Jul 2026
Available online 7 Aug 2026

ABSTRACT: To enhance the mechanical properties of coal gangue ceramsite (CGC) proppants, a technology combining epoxy resin (EP) coating with silane coupling agent KH-792 was employed. Fourier transform infrared (FTIR) analysis confirms that while the epoxy resin forms a physical coating on the ceramsite surface, KH-792 participates in interfacial chemical reactions to construct a dense and rigid siloxane cross-linked network. Studies have shown that coal gangue proppants treated with silane coupling agent were greatly improved in terms of density, crushing rate, turbidity, and water absorption. The CGC proppants modified with a silane coupling agent display the best overall performance. Compared with the untreated CGC proppants, its bulk density falls from 1.56 g/cm^3 to 1.43 g/cm^3 and its apparent density from 2.61 g/cm^3 to 2.43 g/cm^3. Turbidity drops from 65.8 to 10.8 NTU, and 24-h water absorption decreases from 8.8% to 4.8%. Most importantly, the crushing ratio under 69 MPa declines from 3.04% to 2.46%. These improvements have broadened the application prospects of the coal gangue ceramsite proppants in the petroleum industry.

KEYWORDS: coal gangue, proppant, epoxy resin, silane coupling agent, crushing rate

INTRODUCTION

With rising global energy demands, efficient development of unconventional oil and gas resources (e.g., shale gas and tight oil) increasingly depends on hydraulic fracturing technology [1–3]. Proppants serve as critical materials in this technology, maintaining fracture conductivity while directly determining reservoir production capacity and well productivity life [4, 5]. Ideal proppants should exhibit low density, high strength, low crushing rates, excellent water resistance, and thermal stability to withstand complex subsurface environments featuring high temperature, high pressure, and fluid erosion [6]. Although widely used, traditional quartz sand and sintered bauxite proppants face limitations including high density, inadequate mechanical properties, and elevated costs [7, 8]. Consequently, developing novel proppants that combine high performance with cost-effectiveness and environmental benefits has emerged as an active research focus [9].

Coal gangue, a primary solid waste from coal mining and washing operations, not only occupies significant land resources during storage but also poses environmental pollution and geological hazard risks [10, 11]. Nevertheless, its high silicon and aluminum content (typically >50% combined SiO_2 and Al_2O_3) enables transformation through high-temperature sintering into coal gangue ceramic aggregates (CGC). These aggregates feature quartz and mullite as dominant crystalline phases, offering an economical and eco-friendly base material for proppants [12–16]. However, sintered CGC surfaces exhibit inherent roughness, porosity, microcracks, and structural defects. These characteristics result in inadequate crush resistance, surface spalling propensity (evidenced by elevated turbidity), high water absorption, and susceptibility to particle migration and fracture blockage under high-pressure conditions.

To enhance CGC performance, epoxy resin (EP) coating technology is widely employed [17–19]. The excellent adhesion, chemical inertness, and tunable curing properties of EP enable protective layer formation on ceramic surfaces, improving mechanical properties and media resistance [20, 21]. However, simple physical coating often yields uneven layers, interfacial micropores, or weakened bond strength due to poor organic-inorganic compatibility. This leads to coating spalling and failure under prolonged stress or fluid erosion. Studies indicate silane coupling agents effectively strengthen organic-inorganic interfaces [22–24]. Their hydrolyzed alkoxy groups (e.g., Si—OR) undergo condensation with surface hydroxyls to form Si—O—Si covalent bonds, while terminal active groups (e.g., amines) participate in resin cross-linking. This creates a chemical bridge structure that significantly enhances interfacial bonding strength and coating density. KH-792 ([3-(2-aminoethyl) aminopropyl] trimethoxysilane), a bifunctional coupling agent, demonstrates exceptional modification potential in polymer composites through amino-epoxy reactions [25, 26]. Nevertheless, how silane dosage governs interface structure and

EP-CGC proppant properties—including density, crush resistance, water resistance, and thermal stability—requires systematic investigation.

Building upon this foundation, our groups utilized CGC as the matrix and epoxy resin (EP) as the coating to systematically investigate how KH-792 silane coupling agent dosage regulates the structure and performance of EP-CGC composite proppants. The X-ray fluorescence spectroscopy (XRF), X-ray diffraction (XRD), and scanning electron microscopy (SEM) were used to characterize material composition, crystalline phases, and microstructure. The bulk density, apparent density, and crushing rate of proppant also were evaluated according to industry standard SY/T 5108-2014 (China): Water resistance was quantified through turbidity and 24-h water absorption analysis, while thermal stability was assessed via thermal conductivity and thermogravimetric analysis (TGA). The main purpose of this paper is to systematically analyze the concentration gradient of KH-792 to reveal the micro-mechanism of "chemical bridging" at the resin-ceramic interface and determine its optimal dosage range, thereby providing a theoretical and technical foundation for developing high-performance, low-cost green proppants based on coal gangue and promoting solid waste recycling alongside cost-effective oil and gas extraction.

MATERIALS AND METHODS

Experimental materials

CGC proppant (40–70 mesh) was provided by Xinjiang Ruikewo New Materials Co., Ltd., China. Epoxy resin (QY-E8800) and aromatic amine curing agent (QY-H3002) were bought from Hangmo Jiafa New Materials Co., Ltd., China; Silane coupling agent KH-792 was purchased from Dongguan Kangji Co., Ltd., China; anhydrous ethanol (analytical grade) was bought form Tianjin Zhiyuan Co., Ltd., China.

Preparation of epoxy resin-coated proppants

CGC was washed with deionized water and then dried at 100 °C for 12 h. The dried CGC was immersed in an ethanol/water solution (1:9 v/v) containing 0.5–2.0 wt% KH-792 silane coupling agent (relative to CGC mass). After silane coupling agent was hydrolyzed at 50 °C for 3 h under continuous stirring, the silane coupling agent coated CGC was taken out and dried at 100 °C for 6 h. The modified CGC was added into epoxy resin (EP), including curing agent 593 (at a mass ratio of 3:1), and the mixture was stirred for 20 min.

The curing process was conducted at 80 °C for 1 h and then at 140 °C for 1 h. The obtained samples were labeled as EP-CGC, 0.5% KH-792 EP-CGC, 1.0% KH-792 EP-CGC, 1.5% KH-792 EP-CGC, and 2.0% KH-792 EP-CGC.

Density and crushing rate testing of proppants

The bulk density (ρ_{bulk}, g/cm^3), apparent density (ρ_{p}, g/cm^3), and crushing rate (m'_{pan}, %) of the proppant were determined in accordance with the SY/T 5108-2014 standard. Bulk density and apparent density are calculated using Formulas (1) and (2), respectively. Bulk density is determined using the cylinder method, where a specified mass of proppant (m_{p}) is placed in a cylinder (V_{cyl}) for testing. Apparent density is determined using the density bottle method, where ρ_{l} is the density of the test liquid, $m_{\text{f+l}}$ is the total mass of the density bottle and test liquid, and $m_{\text{f+l+p}}$ is the total mass. The crushing rate test involves placing a certain mass of proppant into the crushing chamber and maintaining a pressure of 69 MPa for 2 min. The crushing rate is calculated using Formula (3), which involves the mass of microparticles, m_{pan}, produced by the crushing of the proppant and the total mass of the proppant, m_{s}. Each test was conducted in five parallel experiments per group, and the results were averaged. The final results are expressed as the mean ($\overline{x}$) ± standard deviation (S), with the error bars in the figures representing the sample standard deviation. The mean and sample standard deviation were calculated according to Eqs. (4) and (5), where n is the number of parallel experiments ($n = 5$) in this study; x_i is the individual test result of the i-th parallel experiment (i.e., the individually measured ρ_{bulk}, ρ_{p}, and m'_{pan}); and $\overline{x}$ is the arithmetic mean of the five test results.

$$\rho_{\text{bulk}} = \frac{m_{\text{p}}}{V_{\text{cyl}}} \tag{1}$$

$$\rho_{\text{p}} = \frac{m_{\text{p}}\rho_{\text{l}}}{m_{\text{f+l}} + m_{\text{p}} - m_{\text{f+l+p}}} \tag{2}$$

$$m'_{\text{pan}} = \frac{m_{\text{pan}}}{m_{\text{s}}} \times 100\% \tag{3}$$

$$\overline{x} = \frac{1}{n}\sum_{i=1}^{n} x_i \tag{4}$$

$$S = \sqrt{\frac{\sum_{i=1}^{n}(x_i - \overline{x})^2}{n-1}} \tag{5}$$

Characterization of proppants

The following methods were used to characterize the proppants: To determine the elemental composition and content of coal gangue clay pellets, 5 g of dried powder was pressed into tablets for XRF (ARL 9900, Thermo Fisher Scientific, USA) analysis. XRD (D8 Advance A25, Brook GmbH, Germany) analysis was performed to identify the phase composition and crystal structure, with a scanning range of 5°–80° at a speed of 8°/min. SEM (Quattro S, Thermo Fisher Scientific) analysis was used to observe surface morphology and microstructure. Fourier transform infrared (FTIR)

spectroscopy (Cary 630, Agilent Technologies, USA) was employed to analyze the surface functional groups of the composite sample strips in reflectance mode, over a wavenumber range of 400 to 4000 cm^{-1}. The turbidity of the proppant was assessed using a turbidity meter (WGZ-1A, Lichen Scientific Instruments, China). Five parallel turbidity tests were conducted at room temperature in accordance with the SY/T 5108-2014 standard, and the average value was taken. To evaluate the water resistance of proppants, water absorption tests were conducted at room temperature by weighing the samples immersed in deionized water at regular intervals to measure changes in mass. To study the thermal properties of proppants, analysis was performed using a thermal conductivity meter (DZDR-S,Nanjing Dazhan Testing Instrument, China), and TG (TGA/DSC-1, Mettler Toledo, Switzerland) testing was conducted under nitrogen protection from room temperature to 800 °C at a heating rate of 10 °C/min.

RESULTS AND DISCUSSION

XRF and XRD analysis

XRF compositional analysis of the CGC is presented in Table 1. The material exhibits a characteristic silicate-aluminate composition dominated by SiO_2 (64.52 wt%) and Al_2O_3 (20.64 wt%), collectively constituting 85.16 wt% of the matrix. Minor constituents, in decreasing order of abundance, include Fe_2O_3, K_2O, Na_2O, CaO, MgO, TiO_2, P_2O_5, and MnO_2.

XRD analysis (Fig. 1a) reveals quartz (SiO_2) as the dominant crystalline phase, consistent with the inherent silica richness of coal gangue. Its thermal stability provides structural integrity through skeletal support. Secondary phases include anorthite ($CaAl_2Si_2O_8$), cordierite ($Mg_2Al_4Si_5O_{18}$), and mullite ($Al_6Si_2O_{13}$). Anorthite formation derives from CaO-Al_2O_3-SiO_2 liquid-phase reactions at elevated temperatures, catalyzed by K_2O/Na_2O fluxing agents [27]. Cordierite crystallizes via MgO-Al_2O_3-SiO_2 solid-state reactions at intermediate temperatures with its layered morphology enhancing mechanical performance [28]. Mullite nucleation signifies high-temperature phase transformation, where acicular intergrowths reinforce compressive strength [29]. Iron and titanium oxides partition between amorphous silicate glass and microcrystalline hematite (Fe_2O_3)/ilmenite ($FeTiO_3$), influencing both coloration and thermal behavior.

FTIR analysis

FTIR spectroscopy (Fig. 1b) confirms the group changes of proppant surface before and after KH-792 modification. The spectrum of raw CGC shows the characteristic Si—O—Si skeleton stretching vibration (∼1154 cm^{-1}), and there is almost no obvious hydroxyl signal around 3430 cm^{-1} [30, 31]. Epoxy resin coating (EP-CGC) significantly alters the spectrum: there are new peaks due to epoxy resin (aliphatic C—H stretching of methylene —CH_2— and methyl —CH_3 at ∼2935 and 2829 cm^{-1} [32], a distinct aromatic C=C skeletal vibration of the benzene ring at ∼1510 cm^{-1}, N—H bending of primary amines from the amine curing agent near ∼1600 cm^{-1}), and the intensity of the free hydroxyl (—OH) broad peak (∼3430 cm^{-1}) increases sharply [33]. The appearance of these organic characteristic peaks directly proves the successful physical coating of epoxy resin on the ceramsite surface. More critically, with the introduction of KH-792, the Si—O—Si vibration peak (∼1154 cm^{-1}) significantly shifts to a higher wavenumber (shorter wavelength direction) [33]. Meanwhile, the benzene ring peak at ∼1510 cm^{-1} becomes even stronger. This blue shift indicates that the silane coupling agent successfully participates in the interfacial chemical reaction, building a denser and more rigid siloxane cross-linked network, and the enhanced aromatic signal further confirms an improved coating integrity and better densification after silane modification.

Density and crushing rate test

Density is a fundamental physical property of proppants. Lower bulk density reduces the proppant mass needed to fill fractures, while lower apparent density slows the settling rate, thereby improving particle suspension and transportability in the fracturing fluid. As shown in Fig. 2, the bulk density of the original CGC proppant is 1.56 g/cm^3, and its apparent density is 2.61 g/cm^3. After coating with EP (forming EP-CGC), these values decrease to 1.47 g/cm^3 (bulk) and 2.47 g/cm^3 (apparent). This represents reductions of 5.8% in bulk density and 5.4% in apparent density compared with the uncoated CGC. This decrease arises from the introduction of lower-density EP and the formation of micro-pores due to insufficient interfacial compatibility between the resin and ceramic particles during the physical coating process. Increasing the amount of the silane coupling agent KH-792 initially further reduces density, followed by an increase. Specifically, within the KH-792 dosage range of 0.5 wt% to 1 wt%, bulk density decreases from 1.45 g/cm^3 to 1.43 g/cm^3 and apparent density from 2.44 g/cm^3 to 2.43 g/cm^3. Compared with EP-CGC (without KH-792), the sample with 1 wt% KH-792 (1% KH-792 EP-CGC) exhibits a 2.7% reduction in bulk density and a 1.6% reduction in apparent density. Relative to the original CGC, the reductions are 8.3% (bulk) and 6.9% (apparent). The mechanism illustrated in Fig. 3 involves the amino groups of KH-792 reacting with epoxy groups in the epoxy resin to form C—N bonds. Subsequently, the silane alkoxy groups (Si—OR) in KH-792 hydrolyze to silanol groups (—SiOH), which then condense with silanol groups (Si—OH) on the CGC surface to form Si—O—Si covalent bonds. This reaction constructs an interfacial bridging network [34], significantly enhancing interfacial adhesion. Improved adhesion promotes

Table 1 XRF analysis results for CGC.

	Coal gangue ceramsite										
Ingredient	SiO_2	Al_2O_3	Fe_2O_3	K_2O	Na_2O	CaO	MgO	TiO_2	P_2O_5	MnO_2	Others
Content (wt%)	64.52	20.64	6.07	2.42	1.85	1.50	1.42	1.10	0.12	0.08	0.28

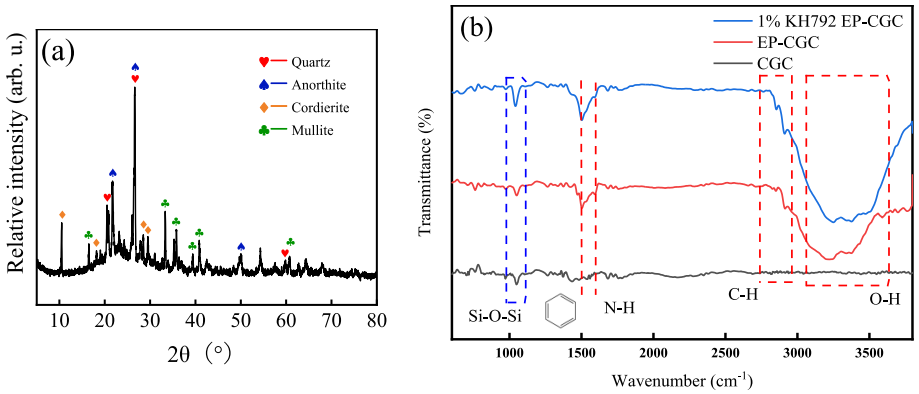

Fig. 1 (a) XRD patterns and (b) FTIR spectra of the raw CGC, EP-CGC, and KH-792-modified proppants.

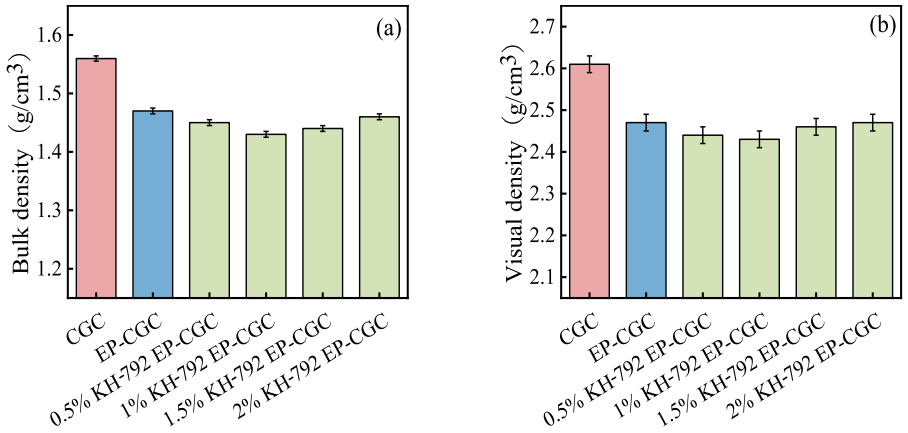

Fig. 2 Effect of silane coupling agent content on the (a) bulk density and (b) apparent density of coal gangue proppants.

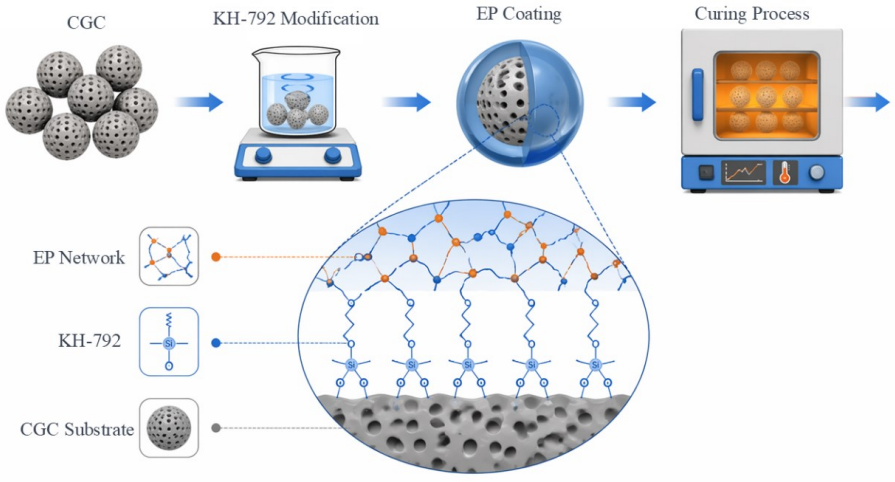

Fig. 3 Schematic diagram of KH-792-modified gangue proppant.

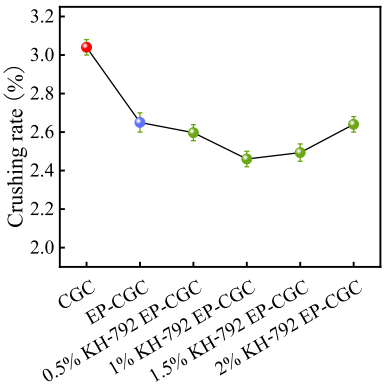

Fig. 4 Effect of silane coupling agent content on the crushing rate of coal gangue proppants.

the formation of a more uniform resin coating, effectively reducing interfacial micro-pores. Concurrently, the intertwining of silane long chains within the epoxy resin crosslinking network induces volume expansion of the resin matrix, contributing to the observed density reduction. However, when the KH-792 addition is increased to 1.5–2 wt%, bulk density recovers to 1.44–1.46 g/cm^3 and apparent density increases to 2.46–2.47 g/cm^3. This reversal beyond the 1.5% additive concentration is attributed to the aggregation of excess self-polymerized Si—O—Si units, which potentially induces micro-cracks, converting closed pores into open pores accessible during pycnometric density measurement. This pore accessibility change reduces the measured volume, consequently increasing the apparent density.

To further illustrate the complete preparation route and the formation of the interfacial "bridge", the fabrication process is schematically presented in Fig. 4. Initially, the raw CGC particles are treated with the silane coupling agent KH-792, during which the alkoxy groups hydrolyze and condense with the hydroxyl groups on the ceramic surface, grafting a silane layer onto the particles via Si—O—Si bonds. The KH-792-modified CGC is then coated with epoxy resin and curing agent; the anchored KH-792 reacts with the epoxy resin, forming covalent C—O—C linkages between the inorganic core and the organic coating. After subsequent curing, a robust KH-792 molecular bridge is established at the ceramic-resin interface, resulting in a tightly bonded epoxy coating on the ceramsite surface.

The crushing rate test provides a direct assessment of proppant mechanical strength, with lower values indicating superior performance. Results of crushing rate are presented in Fig. 4. The crushing rate of the original CGC was 3.04%. After CGC was coated with EP (forming EP-CGC), the crushing rate decreased to 2.65%. This reduction is attributed to the resin layer filling and covering surface defects, combined with its stress-buffering effect. Upon addition of the silane coupling agent KH-792, the crushing rate again further decreased to 2.46% for the 1 wt% KH-792 EP-CGC sample. This represents reductions of 19.1% compared with the original CGC. The reinforcement effect stems from the chemical "resin-ceramic particle" bridge established by KH-792. Specifically, the amino groups of KH-792 cross-link with the epoxy resin, while its silane alkoxy groups (Si—OR) hydrolyze and subsequently condense with surface silanol groups (Si—OH) on the CGC to form Si—O—Si covalent bonds [35]. This significantly enhances interfacial bonding strength, enabling the epoxy resin coating to effectively distribute external loads and inhibit crack propagation. However, when the KH-792 content increased to 2 wt%, the crushing rate rebounded slightly to 2.64%. This increase is attributed to the formation of brittle siloxane products at the interface due to self-polymerization of excess silane [36, 37], coupled with localized stress concentration caused by crosslink density imbalance.

SEM characterization

To better illustrate changes in surface morphology resulting from coating, SEM images of the original CGC proppant, epoxy-coated CGC (EP-CGC), 1 wt% KH-792-modified EP-CGC (1% KH-792 EP-CGC), and 2 wt% KH-792-modified EP-CGC (2% KH-792 EP-CGC) are presented in Fig. 5. The uncoated CGC (Fig. 5a) exhibits a rough and porous surface. Following epoxy resin coating, EP-CGC (Fig. 5b) displays a continuous film layer. However, localized resin agglomeration (indicated by the red frame) and uncovered pores (indicated by the purple frame) are observable, highlighting the limitations of the physical coating process in fully masking surface defects. In contrast, the sample modified with 1 wt% KH-792 (1% KH-792 EP-CGC, Fig. 5c) shows a dense, smooth, and complete coating layer. This improvement results from the chemical bridging facilitated by KH-792, involving dual bonding: Si—O—Si bonds with the ceramic particle surface and C—N bonds (via amino groups) with the EP. Consequently, original cracks and pores are effectively eliminated. Furthermore, the inherent wettability and surface tension of the resin promote self-leveling, ensuring coating uniformity and consistent thickness. However, increasing the KH-792 concentration to 2 wt% (2% KH-792 EP-CGC, Fig. 5d) leads to adverse effects. Excess silane molecules undergo self-condensation, forming flocculent protrusions (highlighted in the yellow box). These protrusions are excessively thick, resulting in the formation of microcracks (denoted by green arrows) and resin cracking (denoted by blue arrows).

Water resistance analysis

Turbidity serves as a key indicator for characterizing the presence of fine particles on proppant surfaces, with the results presented in Fig. 6a. The uncoated

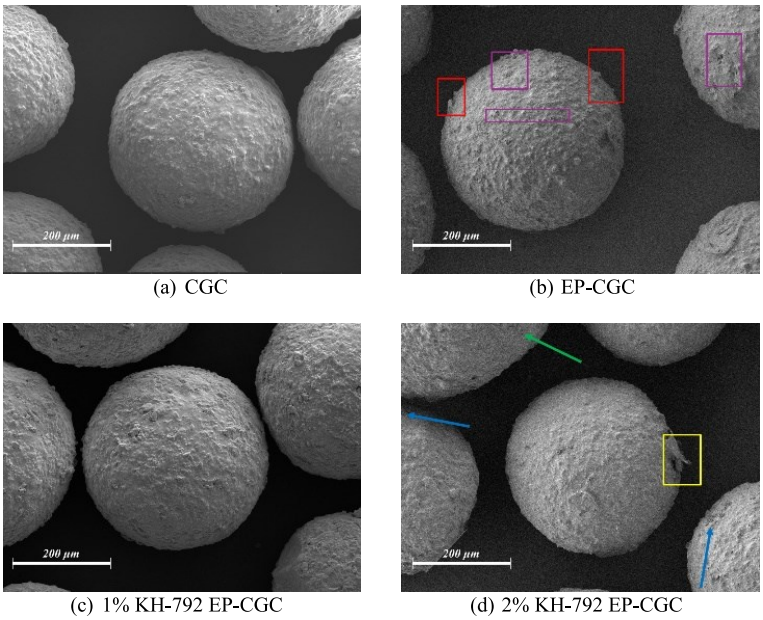

(a) CGC (b) EP-CGC

(c) 1% KH-792 EP-CGC (d) 2% KH-792 EP-CGC

Fig. 5 SEM images of coal gangue proppants with different silane coupling agent contents (a–d).

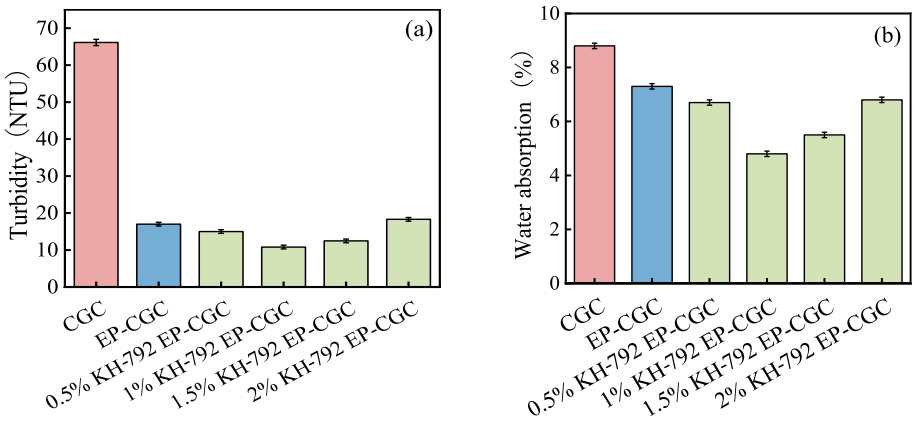

Fig. 6 Effect of KH-792 dosage on the (a) turbidity and (b) 24 h water absorption of the coal gangue proppants.

CGC proppant exhibits a rough, porous surface containing impurities, resulting in a high turbidity of 65.8 NTU. The EP coating (EP-CGC) significantly reduces turbidity to 17 NTU, primarily due to its hydrophobic barrier effect. Turbidity further decreases to 15 NTU for the 0.5 wt% KH-792 EP-CGC sample, attributed to the initial contribution of chemical bonding between the resin and the ceramic particles. When the KH-792 content increases to 1 wt%, the chemical bonding effect dominates the resin-ceramic particle interfacial adhesion in the 1 wt% KH-792 EP-CGC sample. Specifically, the amino groups of KH-792 form covalent bonds with the EP, while its silanol groups react with surface functionalities on the CGC to form a dense Si—O—Si network. This significantly enhances coating integrity, leading to a continued decrease in turbidity to a minimum value of 10.8 NTU. This represents reductions of 36.5% relative to EP-CGC and 83.6% relative to the uncoated CGC. However, when the KH-792 addition is increased to 1.5–2 wt%, turbidity rises to 12.4–18.3 NTU. This increase is caused by excess KH-792, leading to silane self-polymerization that forms brittle protrusions [38, 39] and localized regions of excessively dense crosslinking. These factors induce internal stress and microcracks, which collectively promote the accelerated release of fine particles under hydraulic shear.

Water absorption behavior of the proppant was investigated, with results presented in Fig. 6b. The uncoated CGC proppant exhibits high water absorption (8.8% after 24 h), attributed to capillary action through open pores. Following EP coating (EP-CGC), water absorption decreases to 7.3% (24 h) due to the physical barrier effect of the resin. For

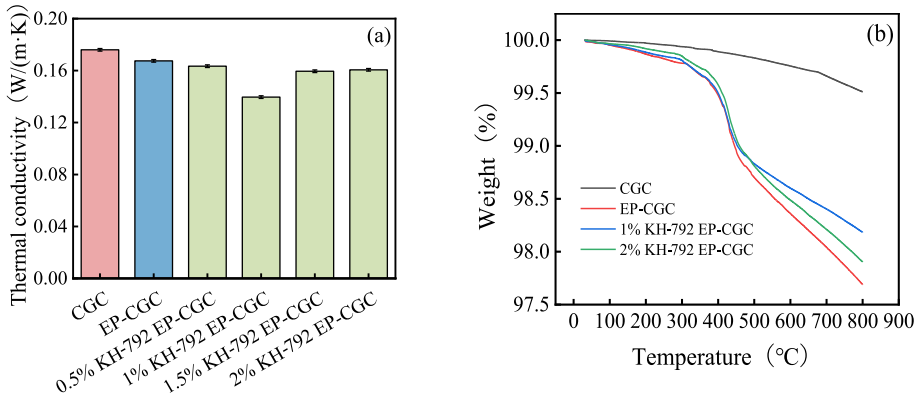

Fig. 7 Thermal properties of the coal gangue proppants. (a) Effect of silane coupling agent content on the thermal conductivity. (b) TG curves of CGC, EP-CGC, and EP-CGC with 1 wt% and 2 wt% KH-792.

the 0.5 wt% KH-792 EP-CGC sample, absorption further declines to 6.7% (24 h), indicating initial effectiveness of chemical bonding and enhanced resin-ceramic interface compaction. At 1 wt% KH-792, chemical bonding dominates interfacial interactions: silanol groups condense with the CGC surface to form a dense Si—O—Si network, while amino groups establish a hydrophobic cross-linked layer with the resin. Consequently, water absorption reduces to 4.8% (24 h), representing decreases of 34.2% relative to EP-CGC and 45.5% relative to uncoated CGC. Importantly, this confirms high interfacial densification. However, at KH-792 concentrations ⩾1.5 wt%, localized over-crosslinking, silane-self-polymerization-induced microcrack networks [38], and residual hydrophilic silanol groups collectively increase water absorption. For 2 wt% KH-792 EP-CGC, absorption rebounds to 6.8%.

Thermal conductivity analysis

To evaluate the effect of KH-792 addition on thermal transfer properties, thermal conductivity measurements were performed (Fig. 7a). The uncoated CGC proppant exhibits a thermal conductivity of 0.1760 W/(m·K). After EP coating, EP-CGC shows reduced conductivity (0.1675 W/(m·K)), primarily due to the inherently low thermal conductivity of the resin. With KH-792 addition, conductivity further decreases significantly: 0.5 wt% KH-792 EP-CGC reaches 0.1634 W/(m·K), while 1.0 wt% KH-792 EP-CGC achieves a minimum value of 0.1396 W/(m·K). This represents reductions of 16.7% relative to EP-CGC and 20.7% relative to uncoated CGC. This trend aligns with microstructural and macro-property evolution. SEM characterization confirms the uniform, intact coating of 1 wt% KH-792 EP-CGC. Its lowest bulk density (1.43 g/cm^3) indicates increased porosity, while minimal 24-h water absorption (4.8%) confirms that these additional pores are predominantly closed. The air trapped within these closed pores creates effective thermal barriers that inhibit conduction [38], explaining the significantly lower thermal conductivity. Conversely, at KH-792 concentrations >1 wt%, conductivity increases substantially: 1.5 wt% KH-792 EP-CGC (0.1595 W/(m·K)) and 2 wt% KH-792 EP-CGC (0.1606 W/(m·K)). This reversal stems from excessive silane coupling agents causing non-uniform resin crosslinking, microcrack formation, and localized heat conduction channels that reduce thermal resistance and promote heat transfer.

To better evaluate the thermal stability of the coated modified proppant, TG testing was performed on CGC, EP-CGC, 1 wt% KH-792 EP-CGC, and 2 wt% KH-792 EP-CGC samples. The results are presented in Fig. 7b. Uncoated CGC exhibits excellent thermal stability due to the inherent inertness of its silico-aluminate matrix, retaining 99.5% of its mass at 800 °C. In contrast, the coated samples displayed decomposition characteristics dominated by the resin component within the 200–800 °C range. An initial slight weight loss occurred from room temperature to approximately 150 °C, primarily attributed to moisture desorption and residual solvent evaporation. The primary decomposition stage commenced at 350 °C, featuring a steep weight loss between 350 °C and 450 °C. This main weight loss phase accounted for up to 33.6% of the total mass loss, corresponding to the scission of molecular main chains (e.g., C—N and C—O bonds) and the formation of volatile products, with the maximum decomposition rate observed at 429 °C. Subsequent secondary decomposition occurred from 450 °C to 800 °C, characterized by a more gradual weight loss resulting from the further cracking of carbonaceous residues formed during the initial stage. At 800 °C, the residual mass for EP-CGC was 97.7%. Increasing the KH-792 content from 0.5 wt% to 1 wt% enhanced thermal stability. Specifically, the residual mass of 1 wt% KH-792 EP-CGC at 800 °C increased to 98.2%, compared with 97.7% for EP-CGC. This improvement arises from the previously confirmed uniform and dense interface, which inhibits thermal decomposition and volatilization, the formation of thermally stable

C—N bonds within the amino-resin, and the protective skeletal effect provided by the Si—O—Si network. The higher residual mass of both 1 wt% and 2 wt% KH-792 EP-CGC compared with unmodified EP-CGC is primarily due to their lower overall organic fraction, which intrinsically decomposes more readily. However, excess KH-792 (2 wt%) reduced the residual mass to 97.9% (compared with 98.2% for 1 wt% KH-792 EP-CGC). While unmodified EP-CGC has the highest organic content and thus the lowest residual mass (97.7%), the decrease for 2 wt% KH-792 EP-CGC correlates directly with the microcracks observed via SEM on the uneven surface, which kinetically accelerated thermal decomposition.

CONCLUSION

KH-792 (1 wt%) synergistically enhances EP-CGC proppants as both a reinforcing agent and pore sealer. FTIR analysis corroborates this dual modification mechanism, confirming the physical encapsulation by the EP and demonstrating that KH-792 participates in interfacial chemical reactions to construct a dense siloxane cross-linked network. The EP forms an effective core-shell structure, reducing crushing rate to 2.46%, representing a 19.1% improvement over uncoated CGC. Simultaneously, KH-792 seals surface defects via chemical bridging, decreasing apparent density to 2.43 g/cm^3 (6.9% lower than that of CGC), water absorption to 4.8% (34.2% reduction from EP-CGC), and thermal conductivity to 0.1396 W/(m·K)—a 20.7% decrease relative to CGC—through trapped insulating air. Critically, exceeding 1 wt% KH-792 triggers silane self-polymerization, generating microcracks that compromise interfacial integrity. Thus, 1 wt% KH-792 optimally balances reinforcement and sealing functions for high-performance proppant design. Ultimately, this optimized approach not only facilitates the sustainable, high-value recycling of coal gangue to mitigate environmental burdens but also provides a highly promising, cost-effective alternative for industrial hydraulic fracturing.

Acknowledgements: This research was funded by the Xinjiang Talent Development Fund (Grant No. XJRC-2025-KJ-PY-KJLJ-015); Special Project for Enhancing the Comprehensive Strength of Disciplines of Yili Normal University (Grant No. 22XKZZ15).

REFERENCES

1. Rezaei A, Siddiqui F, Dindoruk B, Soliman MY (2020) A review on factors influencing the rock mechanics of the gas bearing formations. *J Nat Gas Sci Eng* **80**, 103348.
2. He P, Lu Z, Deng Z, Huang Y, Qin D, Ouyang L, Li M (2023) An advanced hydraulic fracturing technique: Pressure propagation and attenuation mechanism of step rectangular pulse hydraulic fracturing. *Energy Sci Eng* **11**, 299–316.
3. Ali M, Jarni HH, Aftab A, Ismail AR, Saady NMC, Sahito MF, Keshavarz A, Iglauer S, et al (2020) Nanomaterial-based drilling fluids for exploitation of unconventional reservoirs: A review. *Energies* **13**, 3417.
4. Li J, He S, Wu M (2024) A new type microproppant and its property evaluation for shale gas reservoirs. *SPE J* **29**, 346–361.
5. Tang H, Winterfeld PH, Wu YS, Huang Z, Di Y, Pan Z, Zhang J (2016) Integrated simulation of multi-stage hydraulic fracturing in unconventional reservoirs. *J Nat Gas Sci Eng* **36**, 875–892.
6. Wang G, Ma Q, Ren L, Hou J (2024) A comprehensive review of multifunctional proppants. *ACS Omega* **9**, 44120–44133.
7. Liu Y, Wu L, Guo J, Wu Y, Peng Z (2025) New model to evaluate the impact of quartz sand crushing on fracture conductivity in a proppant monolayer. *Eur J Environ Civ Eng* **29**, 380–398.
8. Yang P, Yan F, Bi S, Zeng Y, Sim LB (2024) Preliminary study on fully replacing bauxite with secondary aluminum ash in ceramsite proppants. *Case Stud Chem Environ Eng* **10**, 101015.
9. Liao Z, Li X, Ge L, Yang Z, Zhu J, Xue Q, Wang H (2022) Lightweight proppants in unconventional oil and natural gas development: A review. *Sustain Mater Technol* **33**, e00484.
10. Liu X (2023) Low-carbon utilization of coal gangue under the carbon neutralization strategy: A short review. *J Mater Cycles Waste Manag* **25**, 1978–1987.
11. He R, Cao P, Chen Y, Zhang K, Li W (2025) Research and application of harmless disposal and landfill technology of coal gangue waste in Shendong mining area. *J Phys Conf Ser* **2941**, 012076.
12. Zhao X, Zhang Z, Li W, Shi Y, Guo X, Zhang X, Xu D, Li W, et al (2023) Basic principle, progress, and prospects of coal gangue ceramic proppants. *Int J Appl Ceram Technol* **20**, 2681–2699.
13. Hao J, Hao H, Gao Y, Li X, Qin M, Wang K (2020) Effect of sintering temperature on property of low-density ceramic proppant adding coal gangue. *Mater Sci* **26**, 94–98.
14. Li G, Ma H, Tian Y, Wang K, Zhou Y, Wu Y, Zou X, Hao J, et al (2017) Feasible recycling of industrial waste coal gangue for preparation of mullite based ceramic proppant. *IOP Conf Ser Mater Sci Eng* **230**, 012020.
15. Wang K, Wang H, Zhou Y, Li G, Wu Y, Hao J, Tian Y (2018) Preparation and characterization of low-cost high-performance mullite-quartz ceramic proppants for coal bed methane wells. *Sci Eng Compos Mater* **25**, 957–961.
16. Duan X, Huang Y, Li Y, Zhang W, Huang Z (2023) Evolution mechanism of pore structure in sintered coal gangue ceramsites. *Ceram Int* **49**, 31385–31395.
17. Fan F, Li FX, Tian SC, Sheng M, Khan W, Shi AP, Zhou Y, Xu Q (2021) Hydrophobic epoxy resin coated proppants with ultra-high self-suspension ability and enhanced liquid conductivity. *Pet Sci* **18**, 1753–1759.
18. Xie X, Niu S, Miao Y, Gao X, Cheng L, Gao F (2019) Preparation and properties of resin coated ceramic proppants with ultra light weight and high strength from coal-series kaolin. *Appl Clay Sci* **183**, 105364.
19. Lu ZH, Lan XP, Yuan Y, Zhou JK, Chen SY, Fan F, Niu YC, Li SZ, et al (2022) Shaly detritus embedded epoxy-resin

coated proppants. *Pet Sci* **19**, 1735–1744.
20. Qu ZQ, Fan JC, Guo TK, Chen M, Wang MJ (2023) Development of the epoxy resin phase change proppant based on the Pickering emulsification technology. *J Phys Conf Ser* **2459**, 012115.
21. Fan JC, Qu ZQ, Guo TK, Qi N, Chen M, Hou J, Ge JJ, Liu XQ, et al (2022) Development of self-generated proppant based on modified low-density and low-viscosity epoxy resin and its evaluation. *Pet Sci* **19**, 2240–2252.
22. Chen L, Teng J, Liu G, Liu Z, Cui X, Bu S (2025) Characterization of organic-inorganic interfaces in silanized cementitious thin spray-on liners. *J Mater Sci* **60**, 4211–4241.
23. Teng J, Chen L, Liu G, Cui X, Cui L, Song S (2025) Effect of silanization on mechanical properties and microstructure of thin spray-on liners with different polymer-cement ratios. *J Build Eng* **99**, 111647.
24. Wang X, Zhai S, Wang K, Xie T (2018) Modification of bonding properties and microstructure of resin-cement interface by coupling agents. *Compos Interfaces* **25**, 27–37.
25. Le Huy CH, Thu TNT (2022) Study on modification of nano silica by [3-(2-Aminoethyl) aminopropyl] trimethoxy silane (KH-792) to reinforce polymer film based on epoxy resin Epon 1001X75. *Mater Res Express* **9**, 075305.
26. Song Y, Li J, Zhang J, Che Z, Hong C, Liu M, Wang Y, Zhang J, (2024) Fluorine-free waterborne polyurethanes modified with bis-amino silane coupling agent: Synthesis and properties. *Mater Today Commun* **39**, 109315.
27. Hosseiny AHM, Najafi A, Khalaj G (2023) Investigation of CaO/MgO on the formation of anorthite, diopside, wollastonite and gehlenite phases in the fabrication of fast firing ceramic tiles. *Constr Build Mater* **394**, 132022.
28. Li S, Bao C, Dong W, Liu R (2022) Phase evolution and properties of porous cordierite ceramics prepared by cordierite precursor pastes based on supportless stereolithography. *J Alloys Compd* **922**, 166295.
29. Zhang Q, Wang Q, Dong B, Wang G, Yuan B, Liang P, Li H (2021) Preparation of porous mullite ceramics consisting of needle-like mullite whiskers. *Adv Appl Ceram* **120**, 262–266.
30. Meng Q, Li K, Zhang S, Ni W, Peng Q (2025) Preparation and sintering mechanism of ceramic proppants with oil-based drill cuttings pyrolysis residues. *Ceram Int* **51**, 6183–6194.
31. Xiong D, Wang C, Huang X (2022) Particular pollutants, physical properties, and environmental performance of porous ceramsite materials containing oil-based drilling cuttings residues. *Environ Sci Pollut Res* **29**, 7202–7213.
32. Zhang P, Li D (2026) PVA-KH792-enhanced composite cementitious material from lead-zinc slag and electroplating sludge: Mechanical performance and heavy-metal immobilization. *Materials* **19**, 1420.
33. Chen S, Wang W, He X, Su Y, Xu H, Wang Y, Oh S K (2025) Mechanical treated natural kapok fiber with Ep through oil-milling process for bio-based modified asphalt: Analysis of ageing resistance and Ep releasing. *Case Stud Constr Mater* **22**, e04582.
34. Taieh NK, Hakeem HS, Kadhim MS, Mejbel MK, Adbullah IT, Al-Attabi R, Muhsen MF, Shahatha SH, et al (2025) Optimizing mechanical performance in woven basalt fibers/epoxy composites: using silane coupling agents to modify epoxy resin for fiber-matrix interface. *J Inorg Organomet Polym Mater* **35**, 680–696.
35. Xing X, Wang B, Liu H, Luo S, Wang S, Wei J, Xu W, Yu Q (2023) The mechanism of silane-grafted sodium polyacrylate on the toughening of slag-based geopolymer: An insight from macroscopic-microscopic mechanical properties. *J Mater Sci* **58**, 8757–8778.
36. Chaiworn P, Duangjai P, Pramukkul P (2023) Effects of convection and segregation generated by granular materials in a pseudo-2D rectangular container under vertical vibration. *ScienceAsia* **49S**, 43–49.
37. Salon MCB, Belgacem MN (2010) Competition between hydrolysis and condensation reactions of trialkoxysilanes, as a function of the amount of water and the nature of the organic group. *Colloids Surf A* **366**, 147–154.
38. Min Z, Hongjie Z, Ling L, Zhengang C (2022) MiR-647 inhibits proliferation and improves apoptosis in cisplatin-treated non-small cell lung cancer via down-regulating IGF2 expression. *ScienceAsia* **48**, 705–710.
39. Torry SA, Campbell A, Cunliffe AV, Tod DA (2006) Kinetic analysis of organosilane hydrolysis and condensation. *Int J Adhes Adhes* **26**, 40–49.
40. Liu H, Zhao X (2022) Thermal conductivity analysis of high porosity structures with open and closed pores. *Int J Heat Mass Transfer* **183**, 122089.